PHOTONICS Research

Broadband quasi-phase matching in a MgO:PPLN thin film

Licheng Ge,[1] Yuping Chen,[1,*] Haowei Jiang,[1] Guangzhen Li,[1] Bing Zhu,[1] Yi'an Liu,[1] and Xianfeng Chen[1,2]

[1]State Key Laboratory of Advanced Optical Communication Systems and Networks, School of Physics and Astronomy, Shanghai Jiao Tong University, Shanghai 200240, China
[2]e-mail: xfchen@sjtu.edu.cn
*Corresponding author: ypchen@sjtu.edu.cn

Received 7 May 2018; revised 30 July 2018; accepted 21 August 2018; posted 23 August 2018 (Doc. ID 330997); published 13 September 2018

Future quantum information networks operated on telecom channels require qubit transfer between different wavelengths while preserving quantum coherence and entanglement. Qubit transfer is a nonlinear optical process, but currently the types of atoms used for quantum information processing and storage are limited by the narrow bandwidth of upconversion available. Here we present the first experimental demonstration of broadband and high-efficiency quasi-phase matching second-harmonic generation (SHG) in a chip-scale periodically poled lithium niobate thin film. We achieve a large bandwidth of up to 2 THz for SHG by satisfying quasi-phase matching and group-velocity matching simultaneously. Furthermore, by changing the film thickness, the central wavelength of the quasi-phase matching SHG bandwidth can be modulated from 2.70 μm to 1.44 μm. The reconfigurable quasi-phase matching lithium niobate thin film provides a significant on-chip integrated platform for photonics and quantum optics.

OCIS codes: (130.3730) Lithium niobate; (310.6845) Thin film devices and applications; (190.2620) Harmonic generation and mixing; (190.4390) Nonlinear optics, integrated optics.

https://doi.org/10.1364/PRJ.6.000954

1. INTRODUCTION

Infrared entangled photons have played an essential role in quantum metrology, computing, and imaging [1–4]. Nonlinear upconversion is a common way to convert infrared light to the visible regime for detection [5–8], but some obstacles still remain. First, the low conversion efficiency [9] leads to weak nonlinear interactions between the entangled photons, which can be enhanced with ultrahigh photon flux by generating broadband entangled pairs [10]. Second, for time-resolved single-photon detection with femtosecond resolution [11], it requires detectors to have a broad bandwidth. Third, a high-brightness and widely tunable single-photon source is significant in quantum interference, which has been achieved by the elimination of spectral entanglement through group velocity matching (GVM) [12,13]. To meet the demand for increasing data rates, it is highly desired for integrated optics to combine all the photonic components including light sources, computing units, modulators, and detectors on a single chip [14,15]. So far, no report has been focused on the realization of tunable broadband second-harmonic generation (SHG) on the chip scale.

Recently, $LiNbO_3$ (LN) thin film has attracted much interest [16,17] and has been commercially developed for electro-optical modulators [18–21] and microdisk resonators [22–24]. Traditional waveguides, such as the proton exchange waveguide, have a small index contrast ($\Delta n = 0.09$) and only support the transverse-magnetic (TM) mode [25]. By using ion implantation and wafer bonding, LN thin films exhibiting high nonlinear and electro-optic coefficients, low intrinsic absorption loss, and large transparent windows as bulk materials have been reported [26]. The good mode confinement is due to the high refractive index contrast between LN and SiO_2 ($\Delta n = 0.75$). Therefore, LN thin film can be a promising candidate for a highly integrated photonic platform with infrared sources and detectors on a single chip. With quasi-phase matching (QPM) technology [27–29], periodically poled lithium niobate (PPLN) is known as a good structure for improving nonlinear interaction efficiency. Besides efficiency, the conversion bandwidth is also important. All the reported LN thin-film-based upconverters have a narrow bandwidth of 50 GHz due to group-velocity mismatching [GVMM, $\delta \neq 0$, see Fig. 1(a)], limiting its applications on broadband upconversion for single-wavelength waves and ultrafast pulses [30–35].

In this work, we demonstrated the first, to our knowledge, tunable broadband upconverter by achieving GVM ($\delta = 0$) on chip-scale periodically poled lithium niobate thin film. GVM can always be satisfied under the same condition as QPM if

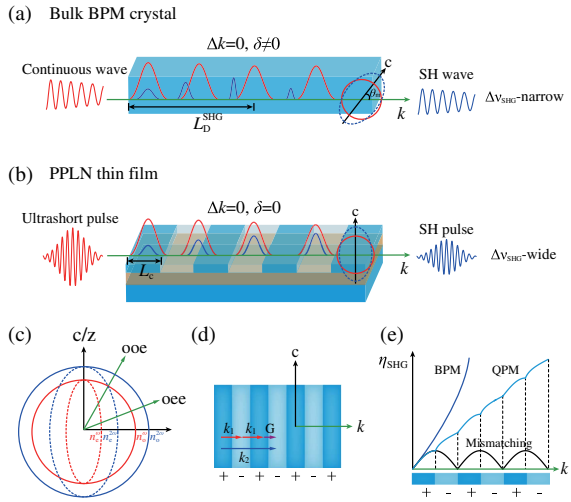

Fig. 1. (a) Traditional GVMM upconversion ($\delta \neq 0$) in bulk birefringent-phase-matching (BPM) crystal has an extremely short interaction length, resulting in low efficiency for the frequency conversion of ultrashort pulses. (b) GVM upconversion ($\delta = 0$) in a PPLN thin film with a wide bandwidth, supporting ultrashort pulse upconversion. L_c is the coherence length. (c) Diagram of birefringent-phase matching of a negative uniaxial crystal. θ_m is the phase-matching angle between optical axis c and wave vector k. (d) Scheme of QPM by offering a reciprocal vector G. (e) The efficiencies of SHG for different phase-matching types.

given a proper QPM period, as introduced in Fig. 1(b). As a result, the bandwidth can be as large as 2 THz. In addition, the dispersion condition for satisfying QPM and GVM simultaneously can be largely modulated from 2.70 μm to 1.44 μm via changing the PPLN film thickness. Our fabricated crystal film supports both transverse-electric (TE) and TM modes [16] so that different types of upconversion are allowed. The dimension of the crystal film can be a few centimeters long, which leads to the great enhancement of conversion efficiency. Experimentally, we observed a $\mathrm{TM}^{\omega} + \mathrm{TM}^{\omega} \rightarrow \mathrm{TM}^{2\omega}$ type broadband upconversion process by using the largest nonlinear coefficient d_{33} (27.2 pm/V). The sample is 4 cm long and has a 700-nm-thick PPLN thin film with a fifth-order QPM period of 20 μm. The measured upconversion bandwidth is 1.875 THz, and the normalized conversion efficiency is 3.3%/W. The efficiency can be enhanced to 82.5%/W theoretically if using the first-order QPM period (4 μm).

2. THEORETICAL ANALYSIS

Supposing v_1 and v_2 are the group velocities of fundamental-frequency (FF) and second-harmonic (SH) waves, the spectral intensity of an SH pulse is expressed as [36]

$$S_2(\omega, L) \propto \mathrm{sinc}^2\{[(v_2^{-1} - v_1^{-1})\omega - \Delta k]L/2\}I_1^2. \quad (1)$$

It shows that the two main factors that affect the spectral bandwidth are group-velocity mismatching ($\delta = v_2^{-1} - v_1^{-1}$) and wave-vector mismatching Δk. L and I_1 are the length of the crystal and the intensity of the FF wave, respectively. Considering $\Delta k = 0$, the GVMM will cause the temporal walk-off effect between the FF and SH pulses. The SHG process will be stopped if the two pulses completely separate in time. The walk-off distance is expressed as $L_D^{\mathrm{SHG}} = \tau_{p1}/|v_2^{-1} - v_1^{-1}|$ [Fig. 1(a)], where τ_{p1} is the pulse width of the FF wave. GVMM can be ignored only when $L \ll L_D^{\mathrm{SHG}}$. The dependence of wave-vector mismatching and GVMM is derived as [37]

$$\frac{\mathrm{d}(\Delta k)}{\mathrm{d}\lambda} = \frac{4\pi c}{\lambda^2}\delta. \quad (2)$$

It shows that GVM ($\delta = 0$) can be achieved in the spectral region where the wave-vector mismatching takes an extremum $[\mathrm{d}(\Delta k)/\mathrm{d}\lambda = 0]$ around which the coherence length (or the QPM period) is nearly constant over a wide wavelength range.

For the QPM upconversion, the wave-vector mismatching is given by $\Delta k = (n^{2\omega} - n^{\omega})4\pi/\lambda - 2\pi/\Lambda$ with the domain period of Λ ($=2L_c$). n^{ω} and $n^{2\omega}$ are the indices of the FF and SH waves. The refractive indices are calculated by Sellmeier equations [38]. In the PPLN thin film, the index should be replaced by the effective refractive index obtained by solving the dispersion relationship of the planar waveguide [39]. Then, the material dispersion is plotted as the relationship between the QPM period (Λ) and the fundamental wavelength (Fig. 2). It has been reported in bulk QPM LN at the telecommunication band by using type-I upconversion (ooe) [30,31,37]. For the famous SHG crystal, the birefringent-phase-matching (BPM) condition of beta barium borate (BBO) can only be satisfied under a specific phase-matching angle θ_m; therefore, it only supports two kinds of SHG, including $\mathrm{o} + \mathrm{o} \rightarrow \mathrm{e}$ and $\mathrm{o} + \mathrm{e} \rightarrow \mathrm{e}$ [see Fig. 1(c)]. The QPM technique [27] used in $LiNbO_3$ can avoid the difficulty of angle-phase matching by offering a reciprocal vector G as shown in Figs. 1(d) and 1(e) and can therefore support several kinds of upconversion processes.

Then we studied the conditions of obtaining simultaneous QPM and GVM in the thin film. For angle-phase-matching SHG in BBO crystal, phase matching (PM) should be satisfied first, where the phase-matching angle θ_m changes monotonously with the FF wavelength. Figure 3 shows the central wavelengths of PM and GVM as a function of θ_m in BBO crystal. GVM and PM can occur simultaneously at $\theta_m = 19.84°$.

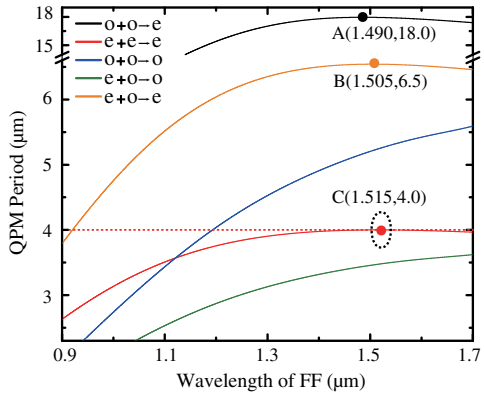

Fig. 2. Simulated QPM period ($2L_c$) as a function of the fundamental wavelength for different types of upconversions. GVM occurs at the extreme of the dispersion curve, in which case it exists in three kinds of upconversion, as marked as points A (1.490, 18.0), B (1.505, 6.5), and C (1.515, 4.0).

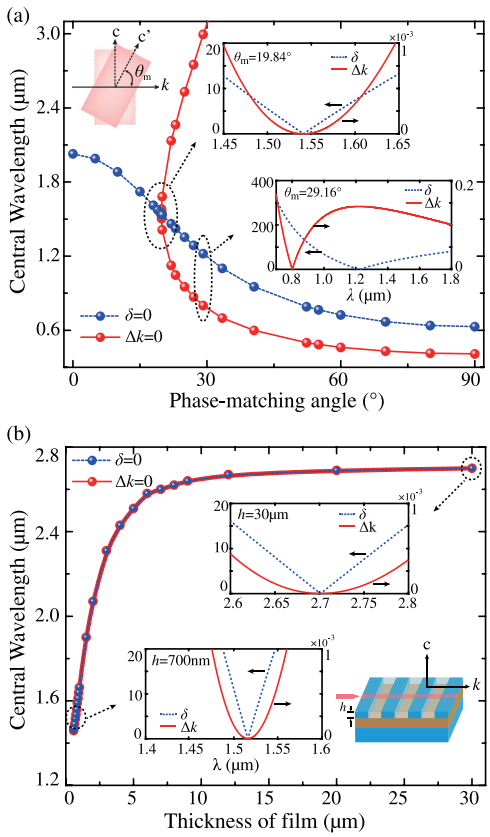

Fig. 3. (a) BBO: central wavelengths of $\delta = 0$ and $\Delta k = 0$ as a function of θ_m. $\delta = 0$ and $\Delta k = 0$ simultaneously only occur at $\theta_m = 19.84°$, as inserted in (a). At other angles, only one matching type can be satisfied. (b) PPLN thin film: central wavelengths of $\delta = 0$ and $\Delta k = 0$ as a function of the thickness of the film. $\Delta k = 0$ can always be satisfied under the same condition when $\delta = 0$ if given a proper QPM period. Insert: two specific examples that show that δ and Δk equal zero at the same time, when $h = 30$ μm at $\lambda = 2.7$ μm (nearly bulk) and $h = 700$ nm at $\lambda = 1.515$ μm, respectively.

At other angles, only one of them is satisfied. For example, for $\theta_m = 29.16°$, $\Delta k = 0$ but $\delta = 187$ fs/mm, which means in order to avoid group-velocity mismatching for 20 fs pulses, the length of the crystal should be less than 107 μm. For PPLN thin film, GVM is automatically satisfied [see Fig. 3(b)]. The change of film thickness will have an impact on the dispersion of the fundamental and second-harmonic waves due to the changes in the efficient refractive index of the thin-film waveguide [40]. As a result, the wavelength for GVM can be tuned by changing film thickness. The modulation range for the central wavelength is as large as 1260 nm (1.44–2.70 μm), corresponding to the film thickness change of 30 μm. The bandwidth of upconversion in PPLN thin film is larger than 2 THz.

3. FABRICATION

Recently, many methods have been proposed and experimentally realized to pole LN film directly [41–43]. Here we fabricated the sample by starting with a periodically poled substrate instead of a single-domain $LiNbO_3$ substrate. First, a z-cut $LiNbO_3$ wafer of 3 inch diameter with 20 μm QPM period is He-ion implanted to a required depth. Another LN handle sample coated by a 2 μm-thickness SiO_2 layer was surface polished to 0.35 nm roughness, enabling direct wafer bonding. The bonded pair of samples is then annealed to improve the bonding strength. By a further increase of the temperature, the sample splits along the He-implanted layer. Afterwards, it is annealed again before the sample surface is polished to 0.5 nm roughness by another chemical mechanical polishing process.

4. EXPERIMENT AND RESULTS

Experimentally, we used a 700-nm-thick, 20 μm-QPM period, and 4-cm-long PPLN thin film to fulfill the GVM upconversion process. Figures 4(a) and 4(b) show the side view scanning electron microscopy (SEM) image and top view optical image of the sample, respectively. Then, a tunable continuous laser (1518–1618 nm) served as the pump source, amplified by erbium-doped fiber amplifiers, where the polarizations were controlled by the polarization controller. The light was then injected to the sample by a lensed fiber, which was set on an XYZ-translation stage with a resolution of 50 nm. The sample was set on YZ-translation stage with a temperature controller at an accuracy of 0.1°C. The output light was collected by a 20× objective lens, and the generated SH wave was monitored by an optical spectrum analyzer (200–1100 nm). We launched a green laser tracer to the sample at the normal direction but observed the light propagation has about 8° misalignment with respect to the x axis [see Fig. 4(b)]. This angle agrees with the QPM grating direction. Since the QPM grating periodically

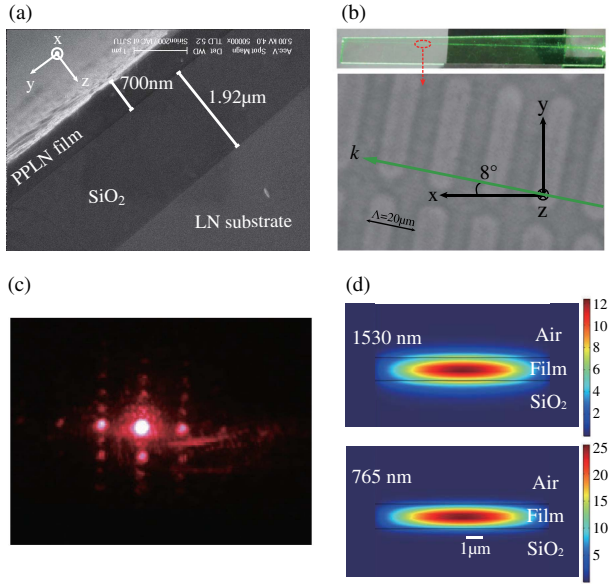

Fig. 4. (a) SEM image of the endface of the sample. A 700-nm-thick PPLN thin film is sitting on a SiO_2 layer with a LN substrate. (b) Observed light confinement and top view of the periodic QPM structure. The direction of the periodic structure has a 8° angle-off with the x axis. (c) Diffraction pattern of PPLN thin film, which indicates the grating structure on the interface of PPLN and SiO_2. (d) Simulated intensity distributions of fundamental and second-harmonic waves with TM mode.

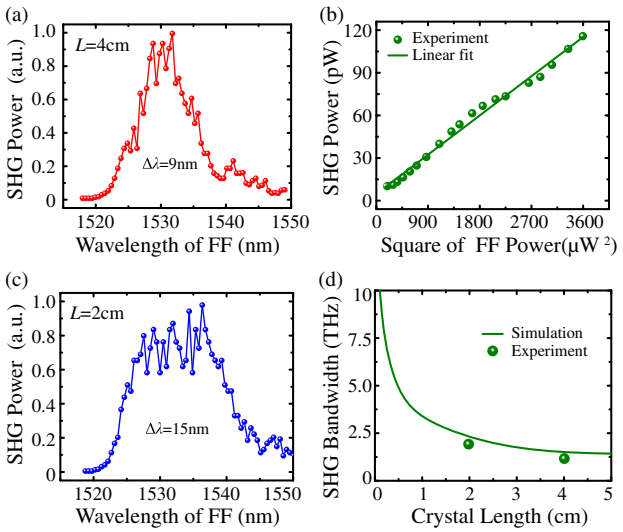

Fig. 5. (a) Measured normalized SHG power as a function of fundamental wavelength. The upconversion bandwidth is 9 nm (1.125 THz) for a 4-cm-long crystal. (b) Linear relationship between SHG power and the square of input FF power at wavelength of 1530 nm and temperature of 24.1°C. (c) Recorded upconversion bandwidth for a 2-cm-long crystal, which is 15 nm (1.875 THz). (d) Experiment and simulation upconversion bandwidths as functions of crystal length.

discontinues along the y axis as well, it proves that light is confined laterally by this discontinuity [44–46]. We can see the diffraction pattern in Fig. 4(c) when a red laser is shot perpendicularly to the surface, which indicates the grating structure on the interface of PPLN film and SiO_2. The COMSOL-simulated intensity distribution of FF and SH waves for the TM mode is plotted in Fig. 4(d). With a QPM period of 20 μm, our sample only supports e + e → e type GVM upconversion (red line and point C in Fig. 2) at the decreased fifth-order QPM conversion efficiency. The optimized temperature for GVM upconversion at the wavelength of 1530 nm is 24.1°C. We verified that the FF and SH waves propagating in the PPLN thin film are both in TM mode. The converted SH power is 120 pW at the pump power of 60 μW, leading to the normalized efficiency of 3.3%/W. It is worth noting that the efficiency can be enhanced to 82.5%/W theoretically if using the first-order QPM period (4 μm).

The SH power as a function of FF wavelength is plotted in Fig. 5(a), from which the upconversion bandwidth is calculated to be 9 nm or 1.125 THz. Figure 5(b) demonstrates the linear relationship between the measured SH power and the square of FF power [47]. Reducing the interaction length can further broaden the upconversion bandwidth but will result in lower conversion efficiency. In another experiment, a 2-cm-long sample was tested to provide 15 nm or 1.875 THz bandwidth [see Fig. 5(c)]. We simulated in Fig. 5(d) the theoretical SHG bandwidth as a function of crystal length and compared it with the experimental results. If using 1-cm-long crystal, the bandwidth can be as broad as 3.2 THz. We notice the shift of the experimental central wavelength (1530 nm) from the theoretical value (1515 nm). This is due to the inaccuracy of Sellmeier equations [38] and the idealization of the slab waveguide used in the simulation. The fifth-order QPM used in our experiment results in low conversion efficiency, but it can be improved by fabricating a first-order QPM period of 4 μm.

5. CONCLUSION

In conclusion, we demonstrated the first tunable broadband upconversion on a periodically poled lithium niobate thin film by satisfying group-velocity matching and quasi-phase matching simultaneously. The central wavelength of the upconversion band can be largely tuned from 2.70 μm to 1.44 μm by changing the film thickness. The measured bandwidth is 1.875 THz for a 2-cm-long sample, along with the conversion efficiency of 3.3%/W. The efficiency can be further enhanced by using a first-order QPM period, and the bandwidth can be made broader by using a shorter interaction length. Our demonstration could lead to the integration of infrared sources and detectors on a single chip and other more advanced photonic integration devices that require broadband operation, for example, a flexible wavelength converter, alloptical wavelength broadcast, and $\chi^{(2)}$:$\chi^{(2)}$ cascading all-optical switch.

Funding. National Key R&D Program of China (2017YFA0303700); National Natural Science Foundation of China (NSFC) (11574208).

REFERENCES

1. G. J. Milburn, "Quantum optical Fredkin gate," Phys. Rev. Lett. **62**, 2124–2127 (1989).
2. E. Knill, R. Laflamme, and G. J. Milburn, "A scheme for efficient quantum computation with linear optics," Nature **409**, 46–52 (2001).
3. L.-M. Duan and H. Kimble, "Scalable photonic quantum computation through cavity-assisted interactions," Phys. Rev. Lett. **92**, 127902 (2004).
4. L. Lugiato, A. Gatti, and E. Brambilla, "Quantum imaging," J. Opt. B **4**, S176–S183 (2002).
5. S. Brustlein, E. Lantz, and F. Devaux, "Absolute radiance imaging using parametric image amplification," Opt. Lett. **32**, 1278–1280 (2007).
6. J. S. Dam, C. Pedersen, and P. Tidemand-Lichtenberg, "High-resolution two-dimensional image upconversion of incoherent light," Opt. Lett. **35**, 3796–3798 (2010).
7. M. J. Nee, R. McCanne, K. J. Kubarych, and M. Joffre, "Two-dimensional infrared spectroscopy detected by chirped pulse upconversion," Opt. Lett. **32**, 713–715 (2007).
8. K. Huang, X. Gu, H. Pan, E. Wu, and H. Zeng, "Few-photon-level two-dimensional infrared imaging by coincidence frequency upconversion," Appl. Phys. Lett. **100**, 151102 (2012).
9. J. Falk and Y. See, "Internal cw parametric upconversion," Appl. Phys. Lett. **32**, 100–101 (1978).
10. B. Dayan, A. Pe'er, A. A. Friesem, and Y. Silberberg, "Nonlinear interactions with an ultrahigh flux of broadband entangled photons," Phys. Rev. Lett. **94**, 043602 (2005).
11. O. Kuzucu, F. N. Wong, S. Kurimura, and S. Tovstonog, "Time-resolved single-photon detection by femtosecond upconversion," Opt. Lett. **33**, 2257–2259 (2008).
12. M. Almendros, J. Huwer, N. Piro, F. Rohde, C. Schuck, M. Hennrich, F. Dubin, and J. Eschner, "Bandwidth-tunable single-photon source in an ion-trap quantum network," Phys. Rev. Lett. **103**, 213601 (2009).
13. P. G. Evans, R. S. Bennink, W. P. Grice, T. S. Humble, and J. Schaake, "Bright source of spectrally uncorrelated polarization-entangled photons with nearly single-mode emission," Phys. Rev. Lett. **105**, 253601 (2010).
14. H. Leng, X. Yu, Y. Gong, P. Xu, Z. Xie, H. Jin, C. Zhang, and S. Zhu, "On-chip steering of entangled photons in nonlinear photonic crystals," Nat. Commun. **2**, 429 (2011).

15. H. Jin, F. Liu, P. Xu, J. Xia, M. Zhong, Y. Yuan, J. Zhou, Y. Gong, W. Wang, and S. Zhu, "On-chip generation and manipulation of entangled photons based on reconfigurable lithium-niobate waveguide circuits," Phys. Rev. Lett. **113**, 103601 (2014).
16. G. Poberaj, H. Hu, W. Sohler, and P. Guenter, "Lithium niobate on insulator (LNOI) for micro photonic devices," Laser Photon. Rev. **6**, 488–503 (2012).
17. A. Boes, B. Corcoran, L. Chang, J. Bowers, and A. Mitchell, "Status and potential of lithium niobate on insulator (LNOI) for photonic integrated circuits," Laser Photon. Rev. **6**, 488–503 (2018).
18. H.-C. Huang, J. I. Dadap, G. Malladi, I. Kymissis, H. Bakhru, and R. M. Osgood, "Helium-ion-induced radiation damage in $linbo_3$ thin-film electro-optic modulators," Opt. Express **22**, 19653–19661 (2014).
19. L. Cai, Y. Kang, and H. Hu, "Electric-optical property of the proton exchanged phase modulator in single-crystal lithium niobate thin film," Opt. Express **24**, 4640–4647 (2016).
20. A. Rao, A. Patil, P. Rabiei, A. Honardoost, R. DeSalvo, A. Paolella, and S. Fathpour, "High-performance and linear thin-film lithium niobate Mach–Zehnder modulators on silicon up to 50 GHz," Opt. Lett. **41**, 5700–5703 (2016).
21. C. Wang, M. Zhang, B. Stern, M. Lipson, and M. Lončar, "Nanophotonic lithium niobate electro-optic modulators," Opt. Express **26**, 1547–1555 (2018).
22. C. Wang, M. J. Burek, Z. Lin, H. A. Atikian, V. Venkataraman, I. Huang, P. Stark, and M. Lončar, "Integrated high quality factor lithium niobate microdisk resonators," Opt. Express **22**, 30924–30933 (2014).
23. J. Lin, Y. Xu, Z. Fang, M. Wang, J. Song, N. Wang, L. Qiao, W. Fang, and Y. Cheng, "Fabrication of high-Q lithium niobate microresonators using femtosecond laser micromachining," Sci. Rep. **5**, 8072 (2015).
24. R. Luo, H. Jiang, H. Liang, Y. Chen, and Q. Lin, "Self-referenced temperature sensing with a lithium niobate microdisk resonator," Opt. Lett. **42**, 1281–1284 (2017).
25. J. Sun and C. Xu, "466 mW green light generation using annealed proton-exchanged periodically poled MgO:$LiNbO_3$ ridge waveguides," Opt. Lett. **37**, 2028–2030 (2012).
26. M. M. Fejer, G. A. Magel, D. H. Jundt, and R. L. Byer, "Quasi-phase-matched second harmonic generation: tuning and tolerances," IEEE J. Quantum Electron. **28**, 2631–2654 (1992).
27. J. Armstrong, N. Bloembergen, J. Ducuing, and P. Pershan, "Interactions between light waves in a nonlinear dielectric," Phys. Rev. **127**, 1918–1939 (1962).
28. H. S. Chan, Z. M. Hsieh, W. H. Liang, A. H. Kung, C. K. Lee, C. J. Lai, R. P. Pan, and L. H. Peng, "Synthesis and measurement of ultrafast waveforms from five discrete optical harmonics," Science **331**, 1165–1168 (2011).
29. Y.-Q. Qin, C. Zhang, Y.-Y. Zhu, X.-P. Hu, and G. Zhao, "Wave-front engineering by Huygens-Fresnel principle for nonlinear optical interactions in domain engineered structures," Phys. Rev. Lett. **100**, 063902 (2008).
30. M. Gong, Y. Chen, F. Lu, and X. Chen, "All optical wavelength broadcast based on simultaneous type I QPM broadband SFG and SHG in MGO:PPLN," Opt. Lett. **35**, 2672–2674 (2010).
31. J. Zhang, Y. Chen, F. Lu, and X. Chen, "Flexible wavelength conversion via cascaded second order nonlinearity using broadband SHG in MGO-doped PPLN," Opt. Express **16**, 6957–6962 (2008).
32. R. Geiss, S. Saravi, A. Sergeyev, S. Diziain, F. Setzpfandt, F. Schrempel, R. Grange, E. B. Kley, A. Tünnermann, and T. Pertsch, "Fabrication of nanoscale lithium niobate waveguides for second-harmonic generation," Opt. Lett. **40**, 2715–2718 (2015).
33. T. Dougherty and E. J. Heilweil, "Dual-beam subpicosecond broadband infrared spectrometer," Opt. Lett. **19**, 129–131 (1994).
34. E. J. Heilweil, "Ultrashort-pulse multichannel infrared spectroscopy using broadband frequency conversion in $LiIO_3$," Opt. Lett. **14**, 551–553 (1989).
35. A. Rao, J. Chiles, S. Khan, S. Toroghi, M. Malinowski, G. F. Camacho-González, and S. Fathpour, "Second-harmonic generation in single-mode integrated waveguides based on mode-shape modulation," Appl. Phys. Lett. **110**, 111109 (2017).
36. C. Rulliere, *Femtosecond Laser Pulses* (Springer, 1998).
37. N. E. Yu, J. H. Ro, M. Cha, S. Kurimura, and T. Taira, "Broadband quasi-phase-matched second-harmonic generation in MGO-doped periodically poled $LiNbO_3$ at the communications band," Opt. Lett. **27**, 1046–1048 (2002).
38. O. Gayer, Z. Sacks, E. Galun, and A. Arie, "Temperature and wavelength dependent refractive index equations for MGO-doped congruent and stoichiometric $LiNbO_3$," Appl. Phys. B **91**, 343–348 (2008).
39. A. W. Snyder and J. Love, *Optical Waveguide Theory* (Springer, 2012).
40. C. Zhu, Y. Chen, G. Li, L. Ge, B. Zhu, M. Hu, and X. Chen, "Multiple-mode phase matching in a single-crystal lithium niobate waveguide for three-wave mixing," Chin. Opt. Lett. **15**, 091901 (2017).
41. L. Chang, Y. Li, N. Volet, L. Wang, J. Peters, and J. E. Bowers, "Thin film wavelength converters for photonic integrated circuits," Optica **3**, 531–535 (2016).
42. R. V. Gainutdinov, T. R. Volk, and H. H. Zhang, "Domain formation and polarization reversal under atomic force microscopy-tip voltages in ion-sliced $LiNbO_3$films on SiO_2/$LiNbO_3$ substrates," Appl. Phys. Lett. **107**, 162903 (2015).
43. P. Mackwitz, M. Rusing, G. Berth, A. Widhalm, K. Müller, and A. Zrenner, "Periodic domain inversion in x-cut single-crystal lithium niobate thin film," Appl. Phys. Lett. **108**, 152902 (2016).
44. S. Kim and V. Gopalan, "Optical index profile at an antiparallel ferroelectric domain wall in lithium niobate," Mater. Sci. Eng. B **120**, 91–94 (2005).
45. I. Mhaouech, V. Coda, G. Montemezzani, M. Chauvet, and L. Guilbert, "Low drive voltage electro-optic Bragg deflector using a periodically poled lithium niobate planar waveguide," Opt. Lett. **41**, 4174–4177 (2016).
46. W. Jin and K. S. Chiang, "Mode switch based on electro-optic long-period waveguide grating in lithium niobate," Opt. Lett. **40**, 237–240 (2015).
47. R. W. Boyd, "Nonlinear optics," in *Handbook of Laser Technology and Applications (Three-Volume Set)* (Taylor & Francis, 2003), pp. 161–183.